A THESIS SUBMITTED TO
THE GRADUATE SCHOOL OF NATURAL AND APPLIED SCIENCES
OF ÇANKIRI KARATEKİN UNIVERSITY

THE SYNTHESIS AND CHARACTERIZATION OF CALCIUM CARBONATE SUPPORTED ZINC OXIDE

IN PARTIAL FULFILLMENT OF THE REQUIREMENTS
FOR
THE DEGREE OF MASTER OF SCIENCE
IN
CHEMICAL ENGINEERING

BY

MAHER JAWAD KADHIM KADHIM

ÇANKIRI

2023

THE SYNTHESIS AND CHARACTERIZATION OF CALCIUM CARBONATE SUPPORTED ZINC OXIDE

By Maher Jawad Kadhim KADHIM

June 2023

We certify that we have read this thesis and that in our opinion it is fully adequate, in scope and in quality, as a thesis for the degree of Master of Science

Advisor **:** Asst. Prof. Dr. Muhammed Bora AKIN

Examining Committee Members:

Chairman **:** Assoc. Prof. Dr. Seyfullah KEYF
Chemical Engineering
Yıldız Technical University

Member **:** Asst Prof. Dr. Muhammed Bora AKIN
Chemical Engineering
Çankırı Karatekin University

Member **:** Asst. Prof. Dr. Zehra Gülten YALÇIN
Chemical Engineering
Çankırı Karatekin University

Approved for the Graduate School of Natural and Applied Sciences

Prof. Dr. Hamit ALYAR
Director of Graduate School

I here by declare that all information in this document has been obtained and presented in accordance with academic rules and ethical conduct. I also declare that, as required by these rules and conduct, I have fully cited and referenced all material and results that are not original to this work.

Maher Jawad Kadhim KADHIM

ABSTRACT

THE SYNTHESIS AND CHARACTERIZATION OF CALCIUM CARBONATE SUPPORTED ZINC OXIDE

Maher Jawad Kadhim KADHIM

Master of Science in Chemical Engineering

Advisor: Asst. Prof. Dr. Muhammed Bora AKIN

June 2023

Calcium carbonate ($CaCO_3$) is a type of chemical compound popularly known as limestone. $CaCO_3$ is abundant in nature, and it has three types of crystal forms, namely aragonite, vaterite and calcite. On the contrary, the crystal form of zinc oxide (ZnO), zincite mineral is rare in nature. ZnO has many uses in fields such as the rubber industry, concrete manufacturing, and medical applications. In addition to all areas of use, its photocatalytic properties and being cheaper than TiO_2, which is an efficient photocatalyst, allowed its use as a catalyst to be investigated. The most important principle of photocatalytic formation is the voids in the crystal structure. These voids will be more abundant in a defective crystal than in a perfect crystal. These gaps can be filled with additives used during crystallization. An excess amount of this substance, also known as an impurity, gives rise to composite materials with new properties such as ZnO/SnO_2, NiO/TiO_2, ZnO/In_2O_3, $p\text{-}ZnO/TiO_2$. In this study, the $CaCO_3$-ZnO composite was synthesized by a hydrothermal process. The size and morphological characteristics of the synthesized composite were characterized by SEM, XRD and BET analyses.

2023, 36 pages

Keywords: Composite, $CaCO_3$, Calcium carbonate, ZnO, Zinc oxide

ÖZET

KALSİYUM KARBONAT DESTEKLİ ÇİNKO OKSİT MALZEME ÜRETİMİ VE KARAKTERİZASYONU

Maher Jawad Kadhim KADHIM

Kimya Mühendisliği, Yüksek Lisans

Tez Danışmanı: Dr. Öğr. Üyesi Muhammed Bora AKIN

Haziran, 2023

Kalsiyum karbonat ($CaCO_3$), halk arasında kireç taşı olarak bilinen bir tür kimyasal bileşiktir. $CaCO_3$ doğada bol miktarda bulunur ve aragonit, vaterit ve kalsit olmak üzere üç tip kristal formu vardır. Aksine, çinko oksitin kristal formu (ZnO), zinkit minerali doğada ender bulunur. Çinko oksit, kauçuk endüstrisi, beton üretimi ve tıbbi uygulamalar gibi alanlarda birçok kullanıma sahiptir. Tüm kullanım alanlarının yanı sıra, fotokatalitik özelliği ve TiO_2'den daha ucuz olması, verimli bir fotokatalizör olması, katalizör olarak kullanımının araştırılmasına olanak sağlamıştır. Fotokatalitik oluşumun en önemli prensibi kristal yapıdaki boşluklardır. Bu boşluklar, kusurlu bir kristalde mükemmel bir kristalden daha bol olacaktır. Bu boşluklar kristalizasyon sırasında kullanılan katkı maddeleri ile doldurulabilir. Safsızlık olarak da bilinen bu maddenin fazlalığı, yeni özelliklere sahip ZnO/SnO_2, NiO/TiO_2, ZnO/In_2O_3, $p\text{-}ZnO/TiO_2$ gibi çeşitli fotokatalizörler gibi kompozit malzemelerin ortaya çıkmasına neden olur. Bu çalışmada $CaCO_3$-ZnO kompoziti hidrotermal proses ile sentezlendi. Sentezlenen kompozitin boyut ve morfolojik özellikleri SEM, XRD ve BET analizleri ile karakterize edildi.

2023, 36 sayfa

Anahtar Kelimeler: Kompozit, $CaCO_3$, Kalsiyum karbonat, ZnO, Çinko oksit

PREFACE AND ACKNOWLEDGEMENTS

I would like to thank the faculty and staff of Çankırı Karatekin University for their efforts with me to complete my studies and obtain a master's degree in chemical engineering. I would also like to thank everyone who helped me, without whom I would not have obtained my master's degree, and the wonderful people I met throughout my studies.

I would like to express my sincere gratitude to my supervisor, Asst. Prof. Dr. Muhammed Bora Akın. For his technical support, insightful guidance, and encouragement during my research. His continued kindness and patience is greatly appreciated. I am very honored to have this opportunity to work with him. He was always there when I needed him, thank you!

I doubt that one day I will be able to convey my full appreciation to my brothers and sisters for their unconditional support, patience, and love, without which I could not have succeeded. Thank you for being by my side all my life.

My deepest appreciation and sincere gratitude go to my wife for her endless love, support, kindness, and encouragement throughout.

To my family who supported me a lot and put up with my shortcomings towards them because of my busyness in my studies, so I dedicate this success to them.

Finally, I also want to thank my current and former friends and colleagues for all the discussions, sharing of knowledge and skills, and for all the fun we've had in the past three years.

Maher Jawad Kadhim KADHIM
Çankırı-2023

CONTENTS

LIST OF SYMBOLS

°C	Degrees Celcius
mol/L	Moles per liters

LIST OF ABBREVIATIONS

4-NP	4-Nitrophenol
AOP	Advanced oxidation process
BET	Brunauer-Emmett-Teller
BPA	Bisphenol A
CB	Conduction band
DRS	Diffuse reflectance UV-Vis spectroscopy
DW	Deionized water
EDX	Energy dispersive X-ray spectroscopy
EIS	Electrochemical impedance spectroscopy
m - LaVO4	The monoclinic phase of Lanthanum vanadate
MB	Methyl blue
MO	Methyl orange
MV	Methyl violet
PL	Photoluminescent
RhB	Rhodamine B
SC	Semiconductor
SEM	Scanning electron microscopy
UV	Ultraviolet
VB	Valence band
Vis	Visible light
XRD	X-ray diffraction

LIST OF FIGURES

LIST OF TABLES

1. INTRODUCTION

Calcium carbonate ($CaCO_3$) polymorphs are chemical compounds that are widely available in nature. Limestone is the common name for calcium carbonate, as it is its main constituent. They have three types of crystalline forms, which are (aragonite, vaterite and calcite). What distinguishes these types is that each of them has different properties. $CaCO_3$ is characterized by good stability and economy.

Calcite is most thermodynamically stable crystalline form, and it is the actual component of limestone. As for the other crystalline forms (aragonite and vaterite), they are transformed into calcite through certain conditions of pressure and temperature, being less stable than calcite in relation to aragonite. As for vaterite, it is not stable.

From an industrial point of view. $CaCO_3$ is used in many fields and is included in many industries such as rubber industry, plastic industry, paints and paper industry, etc. (De Villiers and Materials 1971, Maslen *et al*. 1993, Le Bail *et al*. 2011).

ZnO can be produced through various methods, including:

Direct synthesis: In this method, zinc metal is burned in air to produce zinc oxide.

Precipitation: In this method, a soluble zinc salt (such as zinc nitrate or zinc sulfate) is reacted with an alkali metal hydroxide (such as sodium hydroxide) to form a precipitate of zinc hydroxide. This is then heated to form zinc oxide.

Thermal decomposition: In this method, a zinc compound such as zinc carbonate or zinc hydroxide is heated to high temperatures to decompose it into zinc oxide.

Sol-gel method: In this method, a precursor solution is prepared by dissolving a zinc salt in a solvent, which is then hydrolyzed to form a gel. The gel is then dried and calcined to produce zinc oxide.

ZnO production is an important industrial process due to the wide range of applications of the material in various industries, including cosmetics, rubber, plastics, ceramics, and electronics. The quality of the ZnO produced can vary depending on the production method used and the purity of the starting materials.

ZnO is an inorganic compound in the form of a white powder that is insoluble in water, so it is used as an additive in many products and so on.

The crystalline form ZnO (zincite) is rare in nature, and therefore most of it is produced industrially. ZnO is also a semiconductor whose properties, including its wide bandgap, have made it of interest in many applications (Özgür *et al.* 2005, Battez *et al*. 2008).

ZnO is used in many industries such as rubber industry, concrete manufacturing and medical applications, which allowed its use as a photocatalyst to be investigated (Shifu *et al*. 2006, Shifu *et al.* 2008, Wang *et al*. 2009), and therefore it is very popular with materials scientists, it is considered a suitable substitute for TiO_2, which is considered the most effective photocatalyst, and the reason is that ZnO and TiO_2 have the same bandgap (3.2 eV), but zinc oxide through the experiments of researchers, has proven to be more effective than titanium dioxide, in addition, it is cheaper, safe, non – toxic, chemically stable, environmentally friendly, and easy to manufacture (Pauporte and Rathouský 2007, Qiu *et al*. 2008, Yu *et al*. 2008).

It has also been reported that ZnO is better for producing degradation of organic pollutants due to its high efficiency under visible light (Zhang *et al*. 2012, Mezni *et al*. 2014, Ong *et al*. 2018), and all of this reinforces significantly the photocatalytic process, and its high activity due to the presence of a large number of oxygen vacancies, surface defect, and a

relatively larger reaction rate (Carraway *et al*. 1994, Poulios *et al*. 1999, Pardeshi and Patil 2009, Qamar and Muneer 2009, Ali *et al*. 2010).

Photocatalytic is a modern technology in which light is absorbed by the material to start the oxidation reaction in the environment, that is, it promotes a chemical reaction under visible light irradiation using a catalyst. Where catalysts participate in the reaction and accelerate it and at the end of the reaction remain unchanged (Dalrymple *et al*. 2007), and this means that the proximity of the organic compounds to the surface of the photocatalyst makes it possible for them to decompose under ultraviolet radiation in sunlight or any other light source (for example, artificial light).

Common chemical processes require interaction in which several factors, for example, it needs oxidation agents or reducing agents, or it needs a different medium for the reaction, but its products are dangerous secondary, while the photocatalytic process differs in that the two reactions occur at the same time, and therefore it is considered one of the advanced oxidation processes, where It is currently considered one of the most promising ways to solve environmental problems by sunlight, especially hazardous organic compounds (Yu *et al*. 2008, Nasirian 2017).

The operating and capital costs of any method for treating these compounds are usually expensive and this is considered one of the most important issues in the traditional processes. As for the sphotocatalytic process, the maintenance, design and construction costs are not high and are affordable, with a simple and uncomplicated system like other processes, and the low consumption Detector and low operating time is a measure of increasing the efficiency of any chemical process, and in this process also we need light with energy, and there is no consumption of the chemical reagent (Yu *et al*. 2008).

The adsorbed species on the surface of the catalysts can occur with them reduction and oxidation reaction, as the generation of electron-hole pairs by radiation band gap is what the photocatalytic method depends on (Marci *et al*. 2001).

Among the various semiconductors in the photocatalytic process, titanium dioxide and zinc oxide are excellent photocatalysts. conductors and has a wide band gap (3.2 V), as it can only absorb wavelengths less than 387 nm, and this affects the activity of the process, and that between 3-5% of the solar spectrum is best used.

Also, there are some problems that can be solved by improving the photocatalytic activity, for example, that the performance of zinc oxide for solar energy conversion is affected due to the correlation of optical absorption with large bandwidth power, and we also note that the fast recombination rate of the photogenerated electron-hole pairs of zinc oxide as a photocatalyst is considered a limitation substantial.

Therefore, the main interest of researchers in the recent period has become the subject of changing the optical absorption properties, where the gaps can be provided with the additives used during crystallization. The excessive amount of this substance, also known as impurity, causes the emergence of composite materials with new properties. Many composite photocatalysts such as ZnO/SnO_2, NiO/TiO_2, ZnO/In_2O_3 and p-ZnO/TiO_2 have been synthesized and characterized (Shifu *et al.* 2006, Shifu *et al.* 2008, Wang *et al.* 2009).

1.1 Aim of the study

This study aims at the synthesis and characterization of ($CaCO_3$/ZnO) as a composite photocatalyst. It is planned to use the chemical precipitation method using $Zn(NO_3)_2$, $CaCl_2$, hexamethylenetetraamine and Na_2CO_3.

It will be investigated how the properties of composite materials change afters intering. The investigation of photocatalytic activity after characterization was left dependent on the success of the study.

2. LITERATURE REVIEW

2.1 Composite

Materials are blended in composites in such a way that we may make greater use of their virtues while minimizing the consequences of their weaknesses. This optimisation approach can free a designer from the restrictions connected with the selection and fabrication of traditional materials. He can employ materials that have qualities that can be customized to specific design requirements. Because of the simplicity with which complicated forms may be created, revisiting a conventional design in regard to composites can frequently result in both less expensive and more effective solutions.

Ideally, the qualities of materials for engineering should be repeatable and precise. And, because effective application of the composite principle is dependent on the design flexibility that emerges from adapting the characteristics of multiple kinds of materials to meet a specific purpose, we must also be able to forecast those attributes correctly. Some of the more essential technical features of composites can now be well-predicted using mathematical models, while many cannot (Harris 1999).

2.1.1 Composite semiconductor

The composite of two or more semiconductors is made between two with distinct group holes, successfully separate selections as well as gaps in various types of semiconductors.

Semiconductor coupling can be classified into three states, depending on the relative band gaps and electronic affinity, which are:

Band I, Type II, and Type III alignment

For the first type: for heterojunctions, the generated electrons and holes with narrower band gap The two semiconductors aggregate in the identical semiconductor, thus no Separation of charges enhancement can be anticipated.

In the case of the second category of the heterojunction, charge carrier flow is possible due to the gradient energy band arrangement at the semiconductor interface, which facilitates electron/hole separation.

For the heterojunction of the third type, charge carriers are unable to overcome the disparities in energy found in between the appropriate gaps in the band because They are exceedingly high.

Electrons generated at CB in traditional heterojunctions move from the most negative to the most positive, whereas the holes formed at VB move from the most positive to the other least positive. occurs between the same type of semiconductor (Qiao 2018), and In various types of semiconductors, The separation of both holes and electrons will be effective, resulting in better catalytic performance. Separate into different semiconductors.

Using solgel and solid-state methods by Yang group the new ternary composite SnO_2/ZnO/ TiO_2 was successfully synthesized and used for MO degradation.

The catalytic performance is better compared to semiconductors working alone or any two in combination, by the results obtained from both visible and ultraviolet light, which benefited from the type II interference mainly from the interference.

The combination of TiO_2, SnO_2, and ZnO, meanwhile, can enhance the TiO_2 phase conversion from anatase to rutile, which is more active. Also, the increase in specific surface area was responsible for the rise in catalytic efficiency (Yang *et al*. 2012).

However, only one carrier can be reached, when the semiconductor shell is compactly scattered on the surface of the core, either holes or electrons, on the exterior of the composite, while the other gathers in the center, preventing the degradation process by making a strong carrier transport barrier (Kennedy *et al*. 1997).

In a study by Huang's group this conclusion was substantiated, as the efficiency of ZnO in decomposing methyl orange was reduced due to the ZnS shell layer (Huang *et al*. 2013).

Jie Wang et al. $CaCO_3$-TiO_2 composite was created by co-grinding $CaCO_3$ and TiO_2. The idea l $CaCO_3$-TiO_2 composite, with $CaCO_3$ particle size of 15 μm and TiO_2 mass ratio of 40%, exhibits outstanding catalytic degradation and recovery efficiency towards methyl orange. After 20 and 40 minutes of UV light exposure, the degradation efficiency of the optimum $CaCO_3$-TiO_2 composite was determined to be 90% and 100%, respectively. The deterioration rate is equivalent to that of pure TiO_2 Furthermore, after five cycles, its degrading impact on methyl orange is not greatly decreased.

$CaCO_3$-TiO_2 composites are distinguished by $CaCO_3$ that has been evenly and thoroughly loaded with nano-TiO_2. Loaded TiO_2 disperses considerably better than pure TiO_2, and a strong chemical interaction forms between the $CaCO_3$ and TiO_2 particle surfaces. These are critical processes for increasing the catalytic effectiveness of nano-TiO_2 and decreasing the amount of it in $CaCO_3$-TiO_2 (Wang *et al*. 2019).

2.1.2 Metals or their oxides are used to form the composite

The nanocomposites $CaCO_3$/α-Fe_2O_3 were created. in a single-pot method for producing a cheap and environmentally conscious catalytic oxidation system for the chlorinated volatile organic compound 1,2-dichlorobenzene (o-DCB). In both the presence and absence of water, the activity levels were measured between 200 and 500

degrees celsius. Among the tested catalysts, the nanocomposite containing 9.5 mol% Ca demonstrated the highest activity for catalysis, this might be attributed to the stimulating effect of $CaCO_3$ on α-Fe_2O_3 with smaller crystallite size. The findings from experiments in the absence of water revealed that there had been a regional decrease of catalytic energy around 350 °C due to competing adsorption of water on the locations that were active. The abundance of phenolate, catecholate, o-benzoquinone, carboxylate, and anhydride types of compounds on the outermost layers of the catalysts during the oxidation of o-DCB was demonstrated by in situ FTIR experiments. According to spectral evidence, format entities were more inclined to develop on the surface of 9.5 mol% Ca nanocomposite and subsequently be oxidized to CO, resulting in a higher activity of the catalyst (Ma *et al*. 2013).

On the other hand, doping is the purposeful insertion of impurities, generally ions or atoms, into the inner architectures of a semiconductor. These contaminants are also called as dopants. Depending on the dopants.

2.1.2.1 Metal doping

Metal cations are replaced by Metal ions that are not intrinsics in the semiconductor lattice to accomplish metal doping (Wu *et al*. 2011). To keep a firm, stable solution (Wu *et al*. 2011), as well as excellent solubility (Feng *et al*. 2011), the dopant and original cation sizes should be as close as possible $Cr3^+$, for example, has comparable ionic parameters to Zn^{2+}, implying that $Cr3^+$ may easily enter the ZnO crystal lattice and substitute for Zn^{2+} (Wu *et al*. 2011). Another characteristic that influences the stability of doped semiconductors is valence. A continuous solid solution can be created only if the dopant and starting cation have the identical valences. The difference in valence between Ti^{4+} and W^{6+} caused the development of a limited solid solution when Ti^{4+} was doped into WO_3 particles, Under the given experimental conditions, the solubility of Ti^{4+} dopant was around 10% (Feng *et al*. 2011). Furthermore, because higher adsorption of materials on the catalyst's outermost layer enhances the breakdown of them, doping should be performed near the surface of the semiconductor as well.

Furthermore, because of improved adsorption of precursors on the catalyst surface, doping must occur place near to the surface of the semiconductor In addition. Because of their unoccupied or partially filled atomic orbitals, transition metals (e.g., Cr, W, Mn, Pd, Cu, Ti, Ag, etc.) as well as rare earth metals (e.g., Sn, Ga, Sm, Eu, etc.) are the most extensively used metals in metal doping (Zhao *et al*. 2010). Metal after the changeover (Bi) (Zhong *et al*. 2012) in addition to metal of alkali earth (Sr) (Faisal *et al*. 2014). Dopants can likewise be improve semiconductor catalytic performance. Two typical methods of Metal ion doping has been proposed and experimentally demonstrated:

(i) Adding a level of impurity energy

(ii) Oxygen vacancy growth.

Adding a level of impurity energy

Whenever a different metal ion is doped inside a semiconductor's lattice, atomic orbital hybridization in clean semiconductor conduction band electrons and the metal ion dopant's localized electrons might result in the development between the conduction and valence bands a new level of impurity energy (NIEL) (Wu *et al*. 2011). The NIELs have the ability to behave as electron trappers, donors, or both (Zhao *et al*. 2010, Lazar *et al*. 2012). Meanwhile, on the semiconductor surface, a spatial charge layer will be formed. promoting electron transport and They are prevented from reuniting with holes (Rajneesh *et al*. 2012). Since a consequence, not just may the spectrum of light uptake be enlarged. However, the efficiency of electron/hole separation will be improved. leading to upgraded performance with increasing W dopant concentration, the visible light absorption of ZnO increases (Moafi *et al*. 2013). In the context of Cr-doped ZnO, the sp-d exchange relationships between the generated CB electrons in ZnO and the concentrated d electrons in Cr^{3+} ions that substituted Zn^{2+} ions extended the UV-Visible absorption spectra of non-visible-light-responsive ZnO to virtually the whole visible light spectrum. Exchange interactions with Cr^{3+} and Zn^{2+} led in negative and positive adjustments to CB and VB, accordingly. Under visible light irradiation,

MO TOC removal increased from 5.4% to 58.7%. (Jayanthi *et al*. 2010, Wu *et al*. 2011).

The elements of the initial group (Li, Na, and K) were revealed to act as both acceptors of electrons and contributors in ZnO (Fan *et al*. 2013). By doping K, Zhong et al. dramatically increased decomposition performance towards RhB on ZnO... The K^+ dopants carried out two NIELs between CB and VB concurrently in this system, resulting in a clearly lowered bandgap power and hence a substantially broadened light absorption spectrum (Li *et al*. 2014).

Oxygen vacancy growth

Injection of metal ions into metal oxide semiconductors, this phenomenon happens. Single oxygen vacancy (V_0^+) metal oxide defects have been shown to be capable of trapping holes, resulting in vacancy for charged oxygen (V_0^{++}) defects (Hu and Chen 2007), which subsequently react with OH to give off • OH (Wu *et al*. 2011).

Moafi et al. used a sol-gel technique to dope W^{6+} into ZnO, decreasing ZnO bandgap ranges from 3.2 to 2.85 eV. and increasing Under UV-Vis irradiation, the decomposition performance of MB increased from 49% to 87% in 1 hour. W^{6+} may be replaced or infused interstitially into the ZnO lattice to produce oxygen vacancies, hence speeding the growth of wurtzite ZnO nanocrystallite (Moafi *et al*. 2013).

Other Issues

Metal ion additives may additionally increase semiconductor specific surface area., providing additional areas that are active for substrate adsorption and subsequent breakdown. Aside from lower particle size, which is frequently observed, such as W^{6+} -doped ZnO (Tizro and Kamali 2016), the transformation of semiconductor A further variable influencing enhanced reactive sites and specific surface area is crystal

morphology. Since a consequence of K^+ doping, with lowering size of particle, the ZnO lattice of crystals changed from lamellar to granule form (Li *et al*. 2014).

Catalytic studies revealed that RhB was virtually completely degraded after 3 hours, with a response constant that is 60% greater (Wang *et al*. 2012).

When a semiconductor is doped with foreign metal ions, the degradation mechanism might change. In aqueous solution, for example, MB is quickly dimerized as a thiazine hue. According to one of the previous studies, pure ZnO destroys both MB and its dual MB_2, but W^{6+}-doped ZnO converts MB to $(MB)_2$, prior considerably destroying later. After doping, the deterioration rate increased to 98.6%, yet the bandgap energy stayed almost constant (Voicu *et al*. 2013).

2.1.3 $CaCO_3$/ZnO Composite

Sol-Gel Auto Combustion was used to create $CaCO_3$-ZnO nanoparticles. The hexagonal structure of zinc oxide and trigonal (hexagonal axis) calcium carbonate nanoparticles was seen in the crystalline composition of the manufactured $CaCO_3$-ZnO nanocrystals. The average crystallinity of calcined calcite-zincite is 31.26% without calcination and 30.30% with calcination. The nanoparticles have a 38.07nm average crystal size. without calcination and 39.31 nm after 3-hours of calcination at 500 ℃ (Kumar *et al*. 2020).

On the other hand, the co-precipitation method was utilized to create a highly active $CaCO_3$/ZnO from $(NH_4)_2CO_3$, $Zn(NO_3)_2$, and $Ca(NO_3)_2$ fluorescence emission spectra, the terephthalic acid photoluminescence probing method (TA-PL), UV-vis diffuse reflectance spectroscopy, scanning electron microscopy and X-ray diffraction were used to analyze the composite.The catalytic oxidation of methyl orange and rhodamine B was used to assess the composite's catalytic activity. The findings showed that the composite had much higher catalytic efficiency than pure ZnO. The sample had the best Ca/Zn mole ratio of 1:2 and the greatest TA-PL intensity. The impact of

thermal treatment parameters on the catalytic performance of the composite was investigated. The ideal preparation temperature was around 650 °C for 7 hours. $CaCO_3$/ZnO's photoabsorption wavelength range increases into visible light when compared to pure ZnO, boosting total spectrum efficiency. The various mechanisms of $CaCO_3$ effect on $CaCO_3$/ZnO catalytic activity were also addressed (Chen *et al*. 2011).

2.2 Processes of Precipitation and Crystallization

A solid is created from a supersaturated fluid through the unit processes of precipitation and crystallization. There are several ways to produce the irregular supersaturated state, including solvent loss through evaporation, additional solvent addition, temperature changes, or pressure adjustments, oxidation-reduction reactions, the addition of extra solutes, or possibly a combination of above.

The pace of the process and the size of the solid particles produced typically distinguish crystallization from precipitation Precipitation is a term frequently used to refer to an operation that results in the rapid production of solids, this can lead to minuscule crystals that, while not appearing crystalline to the unaided eye, have extraordinarily distinct x-ray diffraction peaks. In accordance with x-ray diffraction, amorphous solids might additionally form. Precipitation also has a tendency to In contrast to crystallization products, which often may be redissolved using straightforward techniques like heating or dilution, precipitation also refers to a rather irreversible interaction between an added reagent and other species in solution. When solid phases grow quickly and quickly nucleate, precipitation operations frequently start at high supersaturation. Growth, nucleation and supersaturation are the same fundamental processes that take place during crystallization and precipitation. Except at extremely high supersaturation, after achieving a supersaturated condition, nucleation doesn't necessarily start right away, and before to the appearance of the first crystals or solid particles, an induction phase may exist. Nucleation can occur via both homogeneous and heterogeneous mechanisms (Jarvenin 2008).

In recent years, more studies are showing that processes occurring at the molecular and nanometer levels are more complex than previously thought. The traditional model of nucleation and growth frequently fails to accurately reflect the events that occur in truth. clearly, precipitation processes must take into account solid-phase changes, collection processes, and recrystallization phenomena.

Precipitation reactions are important in a variety of goods in industry, including catalysts for precipitation, colors, encrustation preventers, and active component micronization. Numerous instances, the related procedures or items have undergone extensive empirical tuning, it might lead to unintended modifications in the product and, as a consequence, difficult testing to determine a new ideal, especially under shifting production conditions. As a result, precipitation reactions are also of interest to industry in terms of understanding them.

Precipitation reactions can, in theory, be "controlled" with additives. This is the foundation of polymeric encrustation preventers' effectiveness in cleansers and saltwater treatment. These additions maintain low-solubility salts in solution (such as $CaCO_3$) from precipitating both on the heating coils and surfaces of cloth. But the procedures must be understood in order to create the ideal additives it does this by participating in the precipitation (or crystallization) process. Previously, it was widely considered that these chemicals acquire their activity primarily through particular interactions with crystal growth surfaces, as a result, basic comprehension of structure Once more, adjustment during precipitation is necessary. However, only if the processes can be monitored from the beginning of supersaturation (which generates precipitation) to millisecond resolution will a fundamental understanding of structure development in precipitation reactions be possible. For that purpose, matching analytical methods have been devised, allowing for the acquisition of fundamentally new knowledge (Rieger *et al*. 2000).

For a better understanding of the reported results, various features of structure development in $CaCO_3$ precipitation processes are summarized below:

(a) $CaCO_3$ precipitation has been investigated for over a century due to its relevance in both fundamental research (mineralogy, biology, chemistry, geology) and applications (encrustation, pigments, fillers) (Nancollas *et al*. 1971). However, this precipitation is still poorly understood, especially in terms of microscopic mechanisms.

(b) The most stable $CaCO_3$ crystal modification from a thermodynamic standpoint is calcite. Furthermore, $CaCO_3$ has two modifications known as aragonite and vaterite, as well as two hydrate forms and an amorphous state (Clarkson *et al*. 1992).

(c) The initial stage of precipitation is the formation of amorphous $CaCO_3$, which at ambient temperature preferentially transforms to vaterite and subsequently to calcite. This is a famous example of Ostwald's step rule in action (Karpinski and Wey 2002). There is hardly any comprehensive or verified knowledge of the conversion procedures (Rieger *et al*. 2000).

(d) Although calcite is often distinguished by its rhombohedral crystal habit, previous forms commonly appear as beads. Although calcite may be recognized by its tendency of forming rhombohedral crystals, the predecessors commonly appear like beads with diameters of a few micrometers (Söhnel and Mullin 1982, Ogino *et al*. 1987, Brečević and Nielsen 1989). Regarding the intermediary structures, contradictory assertions have been presented. On the one hand, the beads are thought to be constructed of vaterite crystals that were created spherolithically (Tracy *et al*. 1998, Rieger *et al*. 2000). Furthermore, these beads start off amorphous then immediately spherolithically crystallize from the interior out to produce vaterite in contrast (Beniash *et al*. 1999).

(e) These $CaCO_3$ nanoparticles seem to represent fundamental structural elements under various precipitation conditions. interact with the precipitation-affecting additives.

Due to its distinctive physical and chemical characteristics, such as its high electrochemical coupling factor, high chemical stability, good photostability, and wide range of radiation absorption, zinc oxide is a useful material. (Lou *et al*. 1991, Segets *et al*. 2009). Various ways were used to create ZnO particles. The diverse uses of ZnO particles are verified to be dependent on the regulation of physical and chemical features such as size, size dispersity, crystal structure, shape, surface state, dispensability, and organization onto a support (Wahab *et al*. 2007). As a result, a wide range of approaches for manufacturing the molecule have been developed. Hong et al. employed a controlled precipitation approach. The precipitation of using zinc acetate ($Zn(CH_3COO)_2 \cdot H_2O$) and ammonium carbonate ($(NH_4)_2CO_3$), zinc oxide was produced. (Hong *et al*. 2006). Lanje et al., performed a straightforward precipitation process for making zinc oxide. For the cost-effective manufacturing of ZnO particles (Lanje *et al*. 2013), a one step approach with large-scale production without undesirable contaminants is preferred. Wang et al. reported yet another method of regulated zinc oxide precipitation. Precipitation of zinc oxide from solutions of water of NH_4HCO_3 and $ZnSO_4 \cdot 7H_2O$ produced zinc oxide (Wang *et al*. 2010).

2.3 Polymeric additives' effect

Calcium carbonate crystallization studies in the presence of polymeric compounds show that the additions inhibit calcium carbonate precipitation. This impact is stronger for carboxylic polymers than sulfonic polymers and it can be reduced by grafting methoxy poly(ethylene glycol) onto the polymer chain. But $CaCO_3$ deposition can be detected when a little amount is present of Polymeric compounds. Calcite was always the major or only phase that formed. Calcite crystal sizes and morphologies changed morphologies akin to the ones previously demonstrated by calcite interaction with structural intracrystalline constituents were discovered as a function of the polymeric mixtures.

(i) It exhibits how polymeric admixtures modify the rheological characteristics of calcite particles while also changing their habitus.

(ii) It reveals how polymeric admixtures modify calcite particles' habitus and, therefore, their rheological properties.It shows how various calcite crystalline faces may be stabilized by polymeric carboxylate and sulfonate groups; and

(iii) The fact that there are of hydrophilic chains grafted on the primary polymer chain indicates how the aforementioned aspects are connected to polymer conformation and its change Falini *et al*. 2007).

There are several techniques for ZnO production accessible, for example, recently spraying in pyrolysis by ultrasonic procedure was used to create the submicron ZnO crystals. The usage of high heat is the major drawback, they cost money and have temperatures between 200 and 600 °C. Precipitation, microemulsions, sol-gel processes, hydrothermal, and solvothermal synthesis are just a few of the wet chemistry techniques that have made it possible to synthesize a variety of shapes, sizes, and morphologies under controlled conditions at low temperatures. Aqueous precipitation is the most enticing method for possible business growth due to its inexpensiveness and easiness. Once the synthesis circumstances within basic batch reactors have been determined. The separated flow tubular reactor (SFTR), for example, is an innovative reactor that may be used to produce these particles. a continuous method that enables an easy up-scaling from research to production scale without loss in final product quality.

With the application of polymeric additives, it is generally possible to establish better control of the precipitate in terms of size, form, and chemical composition. changing the charge on a particle's surface or adhering to specific crystal planes can both be used to modify crystal formation. Efficient modification of particle size and shape has been achieved during polymer-assisted ZnO production. which produces a range of shapes, including nanorods, hexagonal plates, and particles with a floral appearance (Aimable et al. 2010).

2.4 Initial pH

Polymorph formation is influenced by a variety of factors, includes the pH and additions' type and concentration of additions, the temperature of the solution, the component concentration percentage, supersaturation, and ionic strength. pH of the solution is the most important variable at room temperature, and at different pH values, numerous polymorphs are found. At low pH, when temperatures are high, aragonite predominates as a product. The additive's effects are complex, depends on the type, the concentration, the surroundings in which it is used, and other factors. Depending on the operational circumstances, Supersaturation and concentration proportions have less of an impact on polymorph formation.

To generate useful particulate materials in precipitation processes, controlling operational variables is critical for customizing the crystal form (polymorphism) and shape (morphology), which are relevant to the characteristics and performance of the products if additional processing is to be done. When precipitation occurs as a result of the fast crystallization of a scarcely soluble material with supersaturation caused by a chemical reaction, the operational factors such as solution pH, temperature, solution composition, and the type and quantity of additives must be examined. Among the hardly soluble compounds, calcium carbonate is the most researched system since calcium carbonate precipitation is a common natural phenomenon as well as an important industrial activity. Aragonite, vaterite and calcite are the three crystal types of calcium carbonate that first form.and in polymorphs with variable particle morphologies or shapes. Despite the fact that calcite is more stable than other polymorphs, at room temperature and pressure, precipitates might be a combination of polymorphs or one of the forms predominate. Several experimental techniques for crystal polymorphism and morphology have been developed, including the pH-s method, the MSMPR crystallizer, and the constant-composition approach (Tai and Chen 1998). Anne et al. created zinc oxide particles using water precipitation at 90 °C. The particles were well-crystalline, regular, and round, with a relatively limited size distribution. The impact of pH was also studied. The morphology was outstanding when the pH was increased from slightly acidic to basic conditions. The particles were

transformed from circular nanoparticles to delicately branching flower-like particles with an extended primary crystalline shape.The majority of the research in the literature has been done under simple settings, and the growth process of these structures has been elucidated.

The creation of evenly rounded particles may be related to pH, and the high uniformity in size and shape can be attributed to effective sedimentation route management. The extremely quick mixing (Aimable *et al*. 2010).

3. MATERIALS AND METHODS

3.1 Chemicals Used in the Synthesis of the $CaCO_3$/ZnO Composite

The reactants used in the experiments were chosen to synthesize the compound:

Calcium chloride dihydrate (ACS reagent >99%),

Sodium carbonate (ACS reagent >99.5%),

Zinc nitrate hexahydrate (ACS reagent >99%) and

Sodium hydroxide (ACS reagent >98%).

Calcium chloride dihydrate and sodium carbonate were taken form Iso-Lab Chemical, and the other materials were taken from Sigma-Aldrich (Figure 3.1). Solutions were prepared using deionized water (DW) type II produced by Merck Millipore Elix® Essential Water Purification System in all experiments. The additive Poly(Sodium 4-Styrene Sulfonate) (PSSS) also were taken from Sigma-Aldrich. Molecular weigth of PSSS is about 1.000.000 g/mol.

Figure 3.1 Chemicals used in the synthesis of the $CaCO_3$/ZnO composite

3.2 Method

3.2.1 Composite synthesis method

The solutions of the reactants were prepared using DW, which was prepared using 250 mL of water for each substance and with a concentration of [$CaCl_2$] = [Na_2CO_3] = 0.1 M and [$Zn(NO_3)_2$] = [NaOH] = 0.03 M. In each experiment, the concentration of the PSSS additive was changed between 0-150 mg/L (Table 3.1).

The reactions were carried out by chemical precipitation method, in a jacketed glass reactor with a capacity of 1 liter and with a glass cover. During the experiments, the temperature was kept constant at 25 °C, using a cooled water bath-circulating. After completing the addition of all the reactants, the mixing speed was set to 300 rpm, using a magnetic stirrer (Heidolph MR Hei Tech) in all experiments, and the initial pH value was set to 10. Experimental system is given in Figure 3.2.

Figure 3.2 Laboratory apparatus used in the synthesis of the $CaCO_3$/ZnO composite

After the end of the reaction, the precipitate was filtered by a filter paper and a vacuum pump, thereafter dried after washing in a vacuum oven at 100 °C for about 12 hours.

Table 3.1 Experimental plan

Exp. Code	$[CaCl_2]$= $[Na_2CO_3]$ (mol/L)	$[Zn(NO_3)_2]$=[NaOH] (mol/L)	Additive Concentration (PSSS) (mg/L)
E1	0.1	0.03	-
E2	0.1	0.03	1
E3	0.1	0.03	2.5
E4	0.1	0.03	5
E5	0.1	0.03	10
E6	0.1	0.03	50
E7	0.1	0.03	100
E8	0.1	0.03	150

3.2.2 Characterization of the composite

XRD, SEM and BET analyzes of the obtained powder were made. X-ray diffraction Bruker D8 Discover instrument was used in the investigation of the powder materials. The composite structure was investigated by comparing the scan results with the International Center for Diffraction Data (ICDD) database. 2Theta values ranged from 15° to 90° in XRD analysis scans (Figure 3.3).

SEM microphotographs taken with a Carl Zeiss Sigma 300 VP field emission scanning electron microscope were used to investigate the size and morphology of the synthesized composites (Figure 3.4).

Brunauer–Emmett–Teller (BET) specific surface analyzes were performed using the Quantachrome Nova Touch LX^4 instrument for determination the specific surface area of the synthesized materials. BET specific surface area measurements were made by multi-point nitrogen adsorption isotherm at 77K after degasing the composites with helium flow for 10 hours at 80 °C.

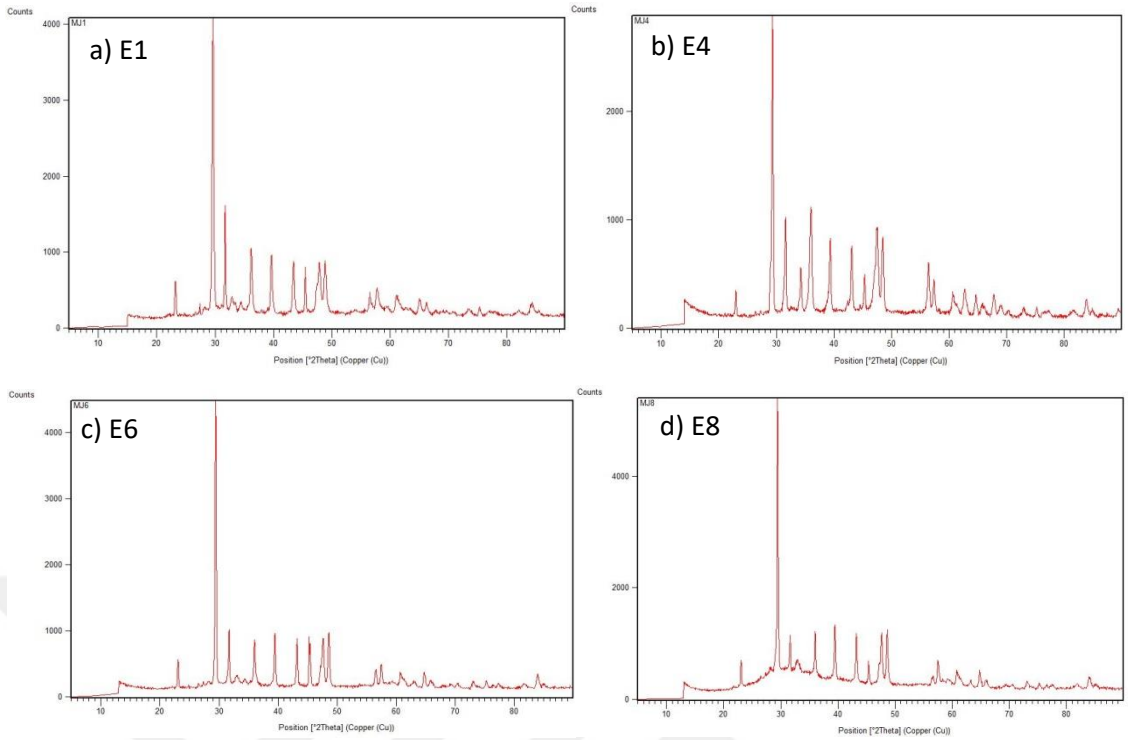

Figure 3.3 Analyses of the composites: (a) No additive, (b) 5 mg/L, (c) 50 mg/L, (d) 150 mg/L

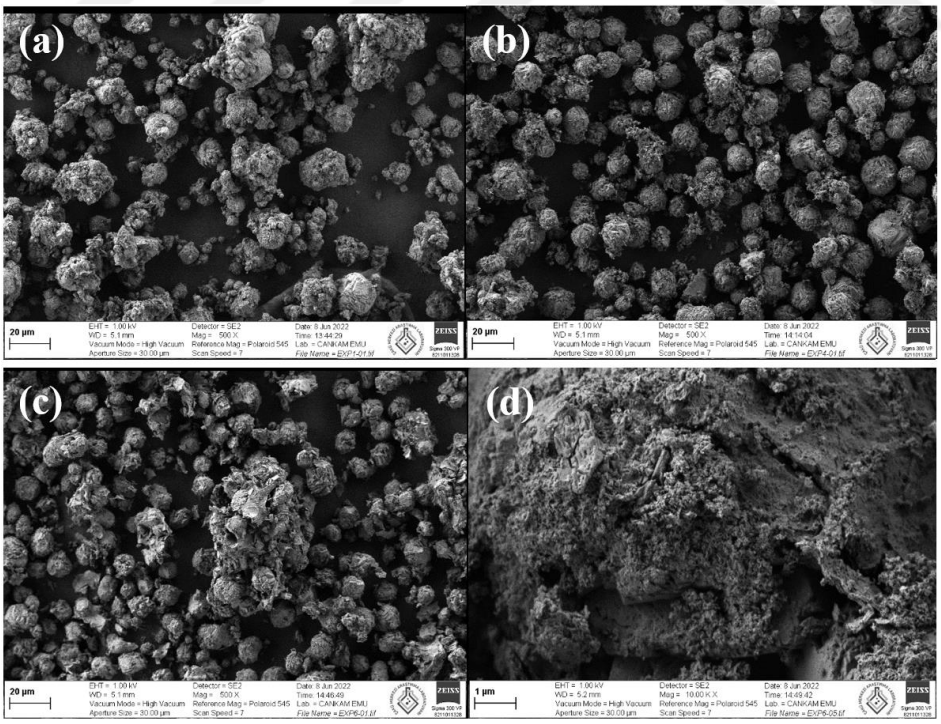

Figure 3.4 SEM micrographs showing the morphology of composite in different additive amount: (a) No additive; (b) 5 mg/L; (c) 50 mg/L; (d) 50 mg/L (higher magnification).

4. RESULTS AND DISCUSSION

4.1 XRD Analysis of the Composite

By examining the powder materials using the Bruker D8 Discover instrument, the composite structure was examined by comparing the scan results with the International Center for Diffraction Data (ICDD) database. Materials without additive, and in the presence of 5 mg/L, 50 mg/L, and 150 mg/L PSSS used calcite/zincite composites were analysed by XRD. 2Theta values ranged from 15° to 90° in XRD analysis scans, the obtained peak values were investigated, and as a result of this investigation, it was determined that calcite/zincite composite were formed (Figure 4.1).

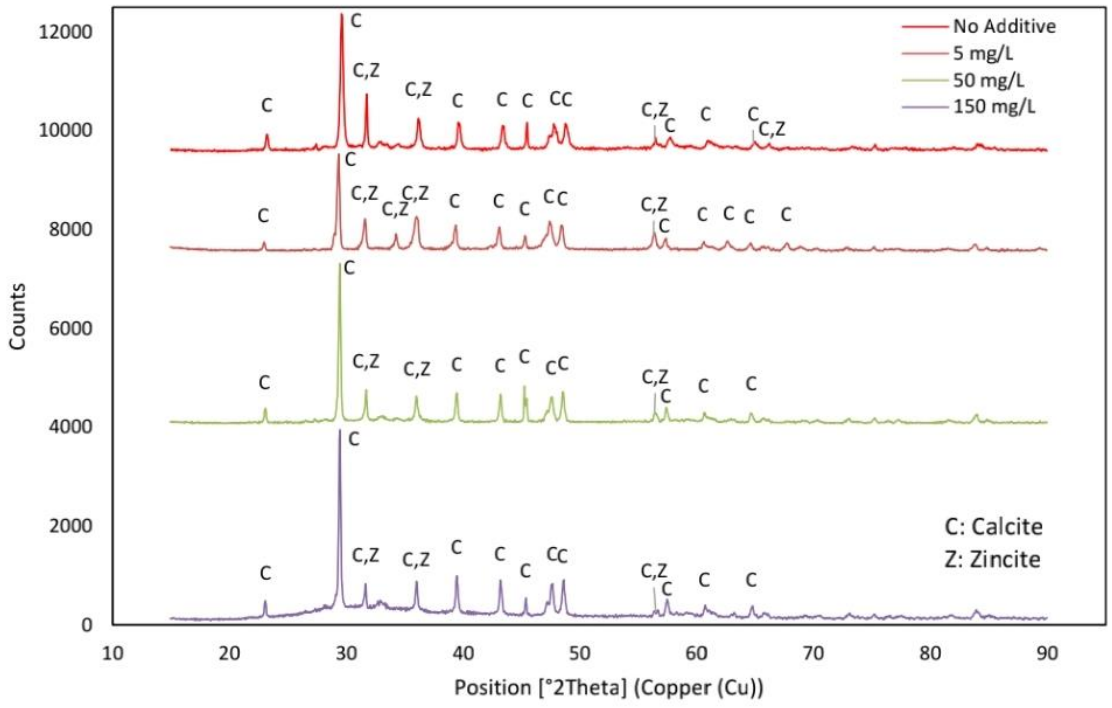

Figure 4.1 XRD analyses of the composites: (a) No additive, (b) 5 mg/L, (c) 50 mg/L, (d) 150 mg/L

As a result of the comparison made from the ICDD database for synthesized materials, it is seen that peaks of the calcite match JCPDS 98-007-9222 and the zincite peaks match JCPDS 98-002-8922.

4.2 SEM Analysis of the Composite

SEM microphotographs taken with a Carl Zeiss Sigma 300 VP field emission scanning electron microscope were used to investigate the size and morphology of the synthesized composites.

In SEM microphotograph analyses, it was seen that calcite/zincite composite material was synthesized in all experiments. In all SEM photographs, it was observed that the calcite crystals surrounded by the zincite crystals, so that the calcite crystals remained embedded and agglomeration occurred in many areas (Figure 4.2). The particles have spherical shape.

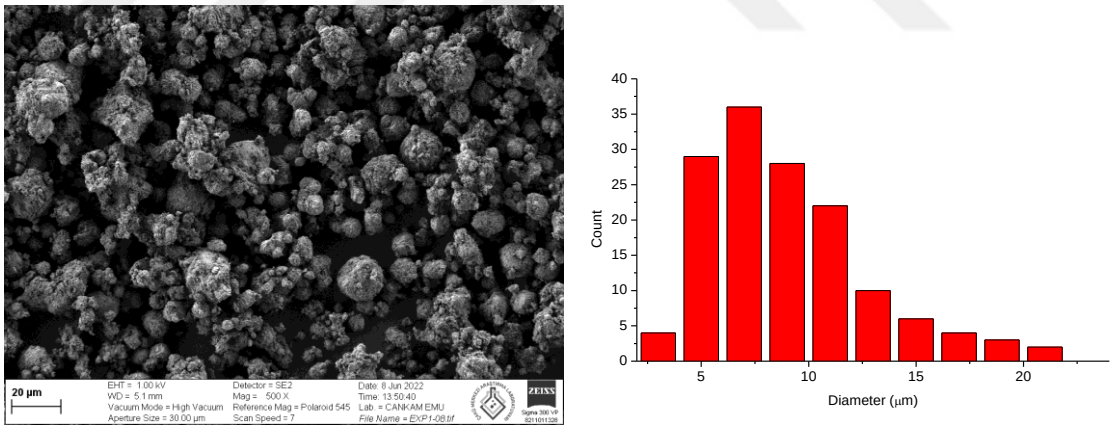

Figure 4.2 Morphology and size distribution of composite without additive

In the SEM images of the material obtained as a result of the experiment without additives, it was seen that the average composite particle size was calculated 8.89 ± 3.82 µm (Table 4.1).

Table 4.1 Descriptive statistics on E1

	N total	Mean	Standard Deviation	Sum	Minimum	Median	Maximum
Diameter	144	8.88774	3.82313	1279.83513	2.71401	8.21814	21.82625

In the SEM images of the material obtained as a result of the experiment performed in the presence of 5 mg/L PSSS, it was seen that the particles were still spherical (Figure 4.3) and the average particle size was calculated as12.77 ± 3.83 µm (Table 4.2).

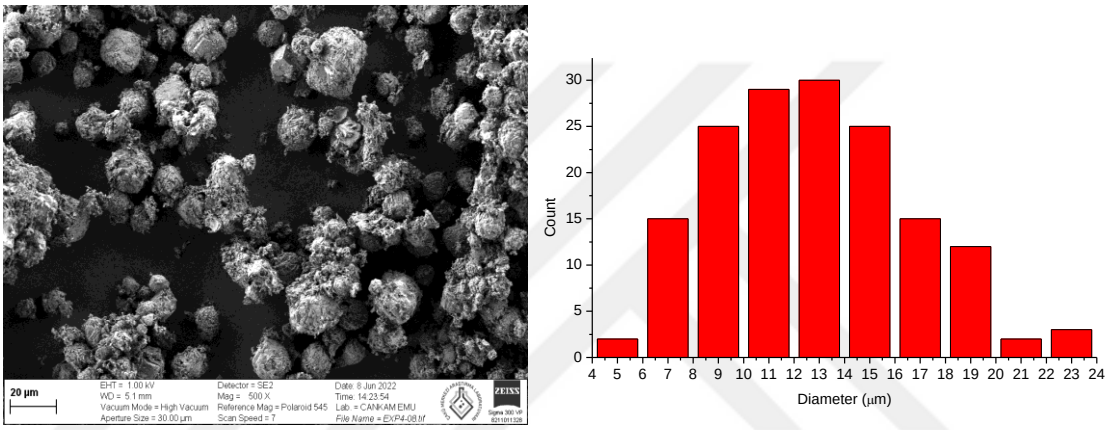

Figure 4.3 Morphology and size distiribution of synthesized composite in the presence of 5 mg/L PSSS.

Table 4.2 Descriptive statistics on E4

	N total	Mean	Standard Deviation	Sum	Minimum	Median	Maximum
Diameter	158	12.77368	3.82658	2018.24162	5.32574	12.5933	23.55471

In the SEM images of the material obtained as a result of the experiment performed in the presence of 50 mg/L PSSS, it was seen that the particles were still spherical (Figure 4.4). But some agglomeration zones show the difference. The average particle size was calculated as 11.12 ± 3.17 µm (Table 4.3).

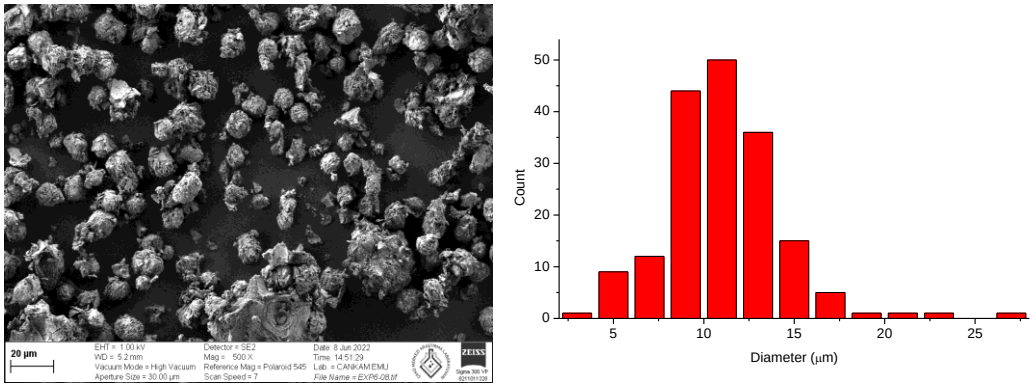

Figure 4.4 Morphology and size distiribution of synthesized composite in the presence of 50 mg/L PSSS.

Table 4.3 Descriptive statistics on E6

	N total	Mean	Standard Deviation	Sum	Minimum	Median	Maximum
Diameter	176	11.1194	3.17295	1957.01473	3.19026	11.01858	27.50801

It was observed that the particles are spherical (Figure 4.5). It is seen that the particles are spherical and approximately 16.06 ± 6.80 µm in diameter (Table 4.4).

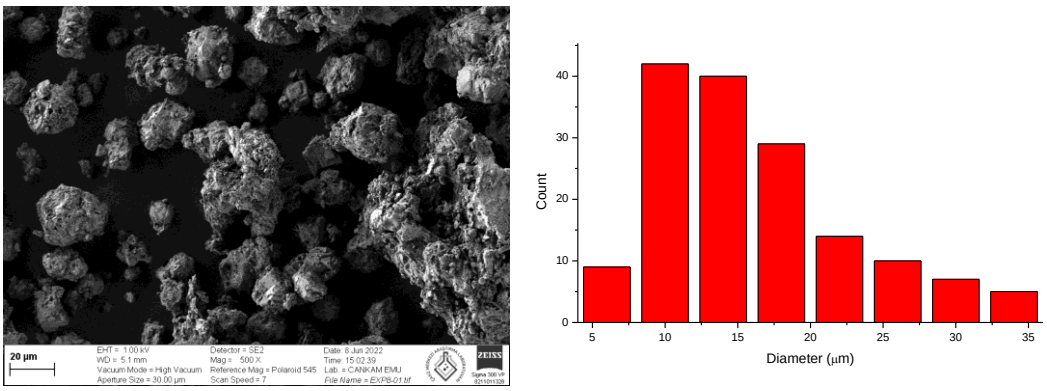

Figure 4.5 Morphology and size distiribution of synthesized composite in the presence of 150 mg/L PSSS.

Table 4.4 Descriptive statistics on E8

	N total	Mean	Standard Deviation	Sum	Minimum	Median	Maximum
Diameter	156	16.09816	6.80096	2511.31326	4.7918	14.15759	34.46509

As seen in Table 4.5, increasing PSSS concentration caused the spheres to increase in diameter.

Table 4.5 Compare of materials' size distribution with descriptive statistics

	Concentration of PSSS (mg/L)	N total	Mean (μm)	Standard Deviation (μm)	Minimum (μm)	Median (μm)	Maximum (μm)
E1	0	144	8.88774	3.82313	2.71401	8.21814	21.82625
E4	5	158	12.77368	3.82658	5.32574	12.5933	23.55471
E6	50	176	11.1194	3.17295	3.19026	11.01858	27.50801
E8	150	156	16.09816	6.80096	4.7918	14.15759	34.46509

In the photographs taken of spheres at higher magnification, it is seen that the spherical forms are obtained with centeral $CaCO_3$ formation wrapped up with the nano-sized ZnO crystals (Figure 4.6).

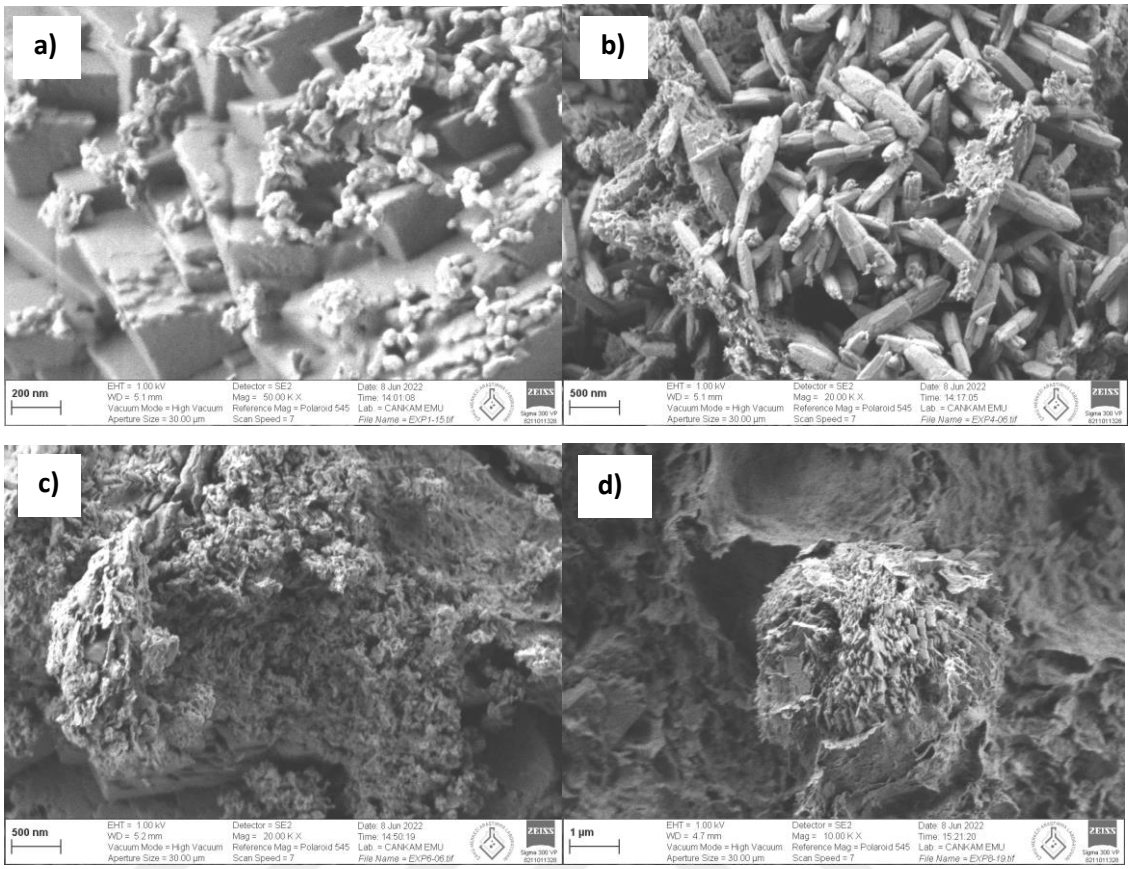

Figure 4.6 SEM micrographs of the nano-sized ZnO crystals: (a) no additive, (b) 5 mg/L (c) 50 mg/L, and 150 mg/L.

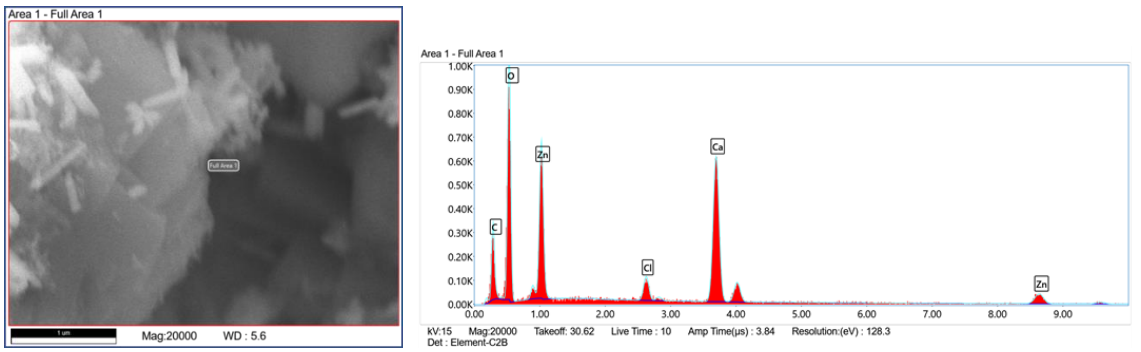

Element	Weight %	Atomic %	Error %	Net Int.	R	A	F
C K	23.83	36.94	13.12	148.76	0.8945	0.1515	1.0000
O K	42.65	49.64	11.15	605.86	0.9068	0.1468	1.0000
Cl K	1.79	0.94	11.08	96.86	0.9436	0.8871	1.0373
Ca K	19.10	8.88	3.78	674.76	0.9533	0.9535	1.0191
Zn K	12.63	3.60	13.49	68.27	0.9844	0.9933	1.0833

Figure 4.7 SEM/EDX analysis of the synthesized material in the presence of 5 mg/L PSSS (E4)

4.3 BET Analysis of the Composite

BET specific surface area measurements were made by multi-point nitrogen adsorption isotherm at 77K after degasing the composites with helium flow for 10 hours at 80 °C.

The BET specific surface area value increase with the increase in the amount of additive due to the increase ZnO crystals synthesized in the presence of additives (Figure 4.8). Although the zincite crystals produced on the composite material are produced in small size, it is thought that the agglomeration behavior on the material affects the BET surface area value. Thus, it can be explained that the increase in the BET surface area stopped after the presence of 5 mg/L additive. In the experiments, the highest BET surface area was obtained as 14.91 m^2/g.

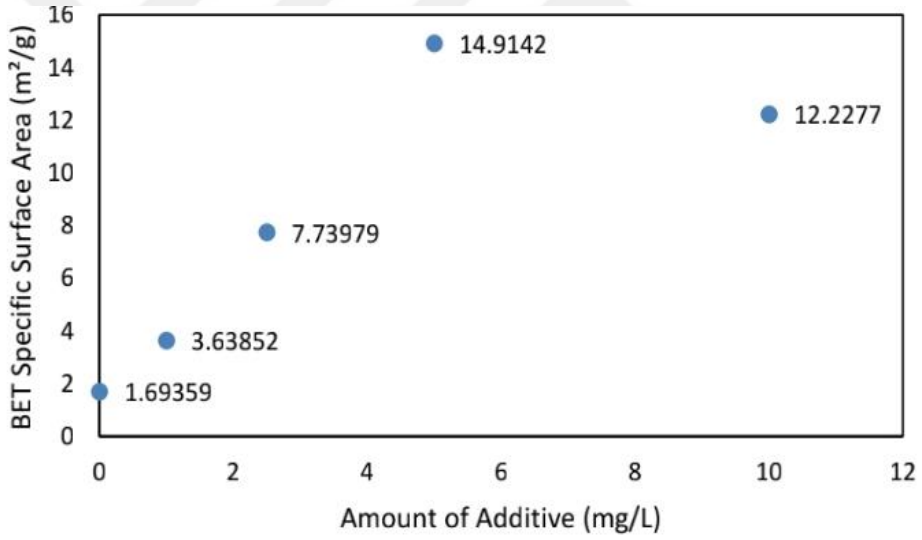

Figure 4.8 Plot of BET specific surface area with amount of additive

5. CONCLUSION

In this research, $CaCO_3$-ZnO composite was synthesized using hydrothermal technique. In the presence of additive, calcium chloride ($CaCl_2$) and sodium carbonate (Na_2CO_3) solutions supported $CaCO_3$ formation, composite synthesis was successful using zinc nitrate hexahydrate ($Zn(NO_3)_2.6H_2O$) and sodium hydroxide (NaOH) in the simultaneous formation of ZnO, and the synthesized composites were characterized by SEM, XRD and BET analyses. Experiments were carried out at 25°C, at a stirring speed of 300 rpm. In experiments, reactant solutions were equimolar and kept $[CaCl_2]=[Na_2CO_3]=0.1$ M and $[Zn(NO_3)_2]=[NaOH]=0.03$ M.

Analysis of all materials synthesized under these conditions showed that $CaCO_3$-ZnO composites were successfully obtained. Increase in crystal size is observed with the increase in the concentration of additive. It was observed that nanosized ZnO crystals accumulated on micron-sized $CaCO_3$ crystals. It was also determined that the BET specific surface area decreased with the increase in amount of additive.

REFERENCES

Aimable, A., Buscaglia, M. T., Buscaglia, V., and Bowen, P. (2010). Polymer-assisted precipitation of ZnO nanoparticles with narrow particle size distribution. Journal of the European Ceramic Society, 30(2), 591-598.

Ali, A. M., Emanuelsson, E. A., and Patterson, D. A. (2010). Photocatalysis with nanostructured zinc oxide thin films: The relationship between morphology and photocatalytic activity under oxygen limited and oxygen rich conditions and evidence for a Mars Van Krevelen mechanism. Applied Catalysis B: Environmental, 97(1-2), 168-181.

Battez, A. H., González, R., Viesca, J. L., Fernández, J. E., Fernández, J. D., Machado, A., and Riba, J. (2008). CuO, ZrO_2 and ZnO nanoparticles as antiwear additive in oil lubricants. Wear, 265(3-4), 422-428.

Beniash, E., Addadi, L., and Weiner, S. (1999). Cellular control over spicule formation in sea urchin embryos: A structural approach. Journal of structural biology, 125(1), 50-62.

Brečević, L., and Nielsen, A. E. (1989). Solubility of amorphous calcium carbonate. Journal of crystal growth, 98(3), 504-510.

Carraway, E. R., Hoffman, A. J., and Hoffmann, M. R. (1994). Photocatalytic oxidation of organic acids on quantum-sized semiconductor colloids. Environmental science & technology, 28(5), 786-793.

Chen, S., Yang, Y., Ji, M., and Liu, W. (2011). Preparation, characterisation and activity evaluation of $CaCO_3$/ZnO photocatalyst. Journal of Experimental Nanoscience, 6(3), 324-336.

Clarkson, J. R., Price, T. J., and Adams, C. J. (1992). Role of metastable phases in the spontaneous precipitation of calcium carbonate. Journal of the Chemical Society, Faraday Transactions, 88(2), 243-249.

Dalrymple, O. K., Yeh, D. H., and Trotz, M. A. (2007). Removing pharmaceuticals and endocrine-disrupting compounds from wastewater by photocatalysis. Journal of Chemical Technology & Biotechnology: International Research in Process, Environmental & Clean Technology, 82(2), 121-134.

De Villiers, J. P. (1971). Crystal structures of aragonite, strontianite, and witherite. American Mineralogist: Journal of Earth and Planetary Materials, 56(5-6), 758-767.

Faisal, M., Ibrahim, A. A., Bouzid, H., Al-Sayari, S. A., Al-Assiri, M. S., and Ismail, A. A. (2014). Hydrothermal synthesis of Sr-doped α-Bi_2O_3 nanosheets as highly efficient photocatalysts under visible light. Journal of Molecular Catalysis A: Chemical, 387, 69-75.

Falini, G., Manara, S., Fermani, S., Roveri, N., Goisis, M., Manganelli, G., and Cassar, L. (2007). Polymeric admixtures effects on calcium carbonate crystallization:

relevance to cement industries and biomineralization. CrystEngComm, 9(12), 1162-1170.

Fan, J. C., Sreekanth, K. M., Xie, Z., Chang, S. L., and Rao, K. V. (2013). p-Type ZnO materials: Theory, growth, properties and devices. Progress in Materials Science, 58(6), 874-985.

Feng, C., Wang, S., and Geng, B. (2011). Ti (iv) doped WO_3 nanocuboids: fabrication and enhanced visible-light-driven photocatalytic performance. Nanoscale, 3(9), 3695-3699.

G. Marci, V. A., M.J. Lopez-Munoz, C. Martin, L. Palmisano, V. Rives, M. Schiavello, R.J.D. Tilley, and A.M. Venezia (2001). Preparation characterization and photocatalytic activity of poly crystalline ZnO/TiO_2 systems. 1. Surface and bulk characterization. J. Phys. Chem B 105 pp. 1026–1032.

Harris, B. (1999). Engineering composite materials. London The Institute of Materials.

Hong, R., Pan, T., Qian, J., and Li, H. (2006). Synthesis and surface modification of ZnO nanoparticles. Chemical Engineering Journal, 119(2-3), 71-81.

Hu, Y., and Chen, H. J. (2007). Origin of green luminescence of ZnO powders reacted with carbon black. Journal of applied physics, 101(12), 124902.

Huang, J., Liu, S., Kuang, L., Zhao, Y., Jiang, T., Liu, S., and Xu, X. (2013). Enhanced photocatalytic activity of quantum-dot-sensitized one-dimensionally-ordered ZnO nanorod photocatalyst. Journal of Environmental Sciences, 25(12), 2487-2491.

Jarvenin, G. (2008). Precipitation and crystallization processes. Consortium for risk evaluation with stakeholder participation (CRESP), 16, 1-14.

Jayanthi, K., Chawla, S., Joshi, A. G., Khan, Z. H., and Kotnala, R. K. (2010). Fabrication of luminescent, magnetic hollow core nanospheres and nanotubes of Cr-doped ZnO by inclusive coprecipitation method. The Journal of Physical Chemistry C, 114(43), 18429-18434.

Karpinski, P. H., and Wey, J. S. (2002). Precipitation processes. In Handbook of industrial crystallization (pp. 141-160). Butterworth-Heinemann.

Kennedy, R., Martini, I., Hartland, G., and Kamat, P. V. (1997). Capped semiconductor colloids: Synthesis and photochemistry of CdS capped SnO_2 nanocrystallites. Journal of Chemical Sciences, 109, 497-507.

Kumar, L. S., Shantha, V., Naik, C., Drakshayani, D. N., Kataraki, P. S., Janvekar, A. A., and Ishak, A. (2020). Synthesis of calcite-zincite nano composite materials using sol-gel auto combustion method. In IOP Conference Series: Materials Science and Engineering, 1003(1), 012132.

Lanje, A. S., Sharma, S. J., Ningthoujam, R. S., Ahn, J. S., and Pode, R. B. (2013). Low temperature dielectric studies of zinc oxide (ZnO) nanoparticles prepared by precipitation method. Advanced Powder Technology, 24(1), 331-335.

Lazar, M. A., Varghese, S., and Nair, S. S. (2012). Photocatalytic water treatment by titanium dioxide: recent updates. Catalysts, 2(4), 572-601.

Le Bail, A., Ouhenia, S., and Chateigner, D. (2011). Microtwinning hypothesis for a more ordered vaterite model. Powder Diffraction, 26(1), 16-21.

Li, D., Huang, J. F., Cao, L. Y., OuYang, H. B., Li, J. Y., and Yao, C. Y. (2014). Microwave hydrothermal synthesis of K^+ doped ZnO nanoparticles with enhanced photocatalytic properties under visible-light. Materials Letters, 118, 17-20.

Lou, X., Shen, H. S., and Shen, Y. S. (1991). Development of ZnO series ceramic semiconductor gas sensors. J. Sens. Trans. Technol, 3(1), 1-5.

Ma, X., Sun, Q., Feng, X., He, X., Guo, J., Sun, H., and Cao, H. (2013). Catalytic oxidation of 1, 2-dichlorobenzene over $CaCO_3$/α-Fe_2O_3 nanocomposite catalysts. Applied Catalysis A: General, 450, 143-151.

Maslen, E. N., Spadaccini, N., Ito, T., Marumo, F., Tanaka, K., and Satow, Y. (1993). A synchrotron radiation study of potassium zinc fluoride perovskite. Acta Crystallographica Section B: Structural Science, 49(4), 632-636.

Mezni, A., Mlayah, A., Serin, V., and Smiri, L. S. (2014). Synthesis of hybrid Au–ZnO nanoparticles using a one pot polyol process. Materials Chemistry and Physics, 147(3), 496-503.

Moafi, H. F., Zanjanchi, M. A., and Shojaie, A. F. (2013). Tungsten-doped ZnO nanocomposite: Synthesis, characterization, and highly active photocatalyst toward dye photodegradation. Materials Chemistry and Physics, 139(2-3), 856-864.

Mohan, R., Krishnamoorthy, K., and Kim, S. J. (2012). Enhanced photocatalytic activity of Cu-doped ZnO nanorods. Solid State Communications, 152(5), 375-380.

Nancollas, G. H., and Reddy, M. M. (1971). The crystallization of calcium carbonate. II. Calcite growth mechanism. Journal of colloid and interface science, 37(4), 824-830.

Nasirian, M. (2017). Development of a Novel Photocatalyst for the Photocatalytic Treatment of Industrial Wastewater, Doctoral dissertation, Ryerson University, Canada.

Ogino, T., Suzuki, T., and Sawada, K. (1987). The formation and transformation mechanism of calcium carbonate in water. Geochimica et Cosmochimica Acta, 51(10), 2757-2767.

Ong, C. B., Ng, L. Y., and Mohammad, A. W. (2018). A review of ZnO nanoparticles as solar photocatalysts: Synthesis, mechanisms and applications. Renewable and Sustainable Energy Reviews, 81, 536-551.

Özgür, Ü., Alivov, Y. I., Liu, C., Teke, A., Reshchikov, M. A., Doğan, S., and Morkoç, A. H. (2005). A comprehensive review of ZnO materials and devices. Journal of applied physics, 98(4), 041301.

Pardeshi, S. K., and Patil, A. B. (2009). Effect of morphology and crystallite size on solar photocatalytic activity of zinc oxide synthesized by solution free mechanochemical method. Journal of Molecular Catalysis A: Chemical, 308(1-2), 32-40.

Pauporte, T., and Rathouský, J. (2007). Electrodeposited mesoporous ZnO thin films as efficient photocatalysts for the degradation of dye pollutants. The Journal of Physical Chemistry C, 111(21), 7639-7644.

Poulios, I., Makri, D., and Prohaska, X. (1999). Photocatalytic treatment of olive milling waste water: oxidation of protocatechuic acid. Global Nest: the Int. J, 1(1), 55-62.

Qamar, M., and Muneer, M. (2009). A comparative photocatalytic activity of titanium dioxide and zinc oxide by investigating the degradation of vanillin. Desalination, 249(2), 535-540.

Qiao, Y. (2018). Preparation, characterization, and evaluation of photocatalytic properties of a novel $NaNbO_3/Bi_2WO_6$ heterostructure photocatalyst for water treatment, Doctoral dissertation, University of Ottawa, Canada.

Qiu, X., Li, L., Zheng, J., Liu, J., Sun, X., and Li, G. (2008). Origin of the enhanced photocatalytic activities of semiconductors: a case study of ZnO doped with Mg^{2+}. The Journal of Physical Chemistry C, 112(32), 12242-12248.

Rieger, J., Thieme, J., and Schmidt, C. (2000). Study of precipitation reactions by X-ray microscopy: $CaCO_3$ precipitation and the effect of polycarboxylates. Langmuir, 16(22), 8300-8305.

Segets, D., Gradl, J., Taylor, R. K., Vassilev, V., and Peukert, W. (2009). Analysis of optical absorbance spectra for the determination of ZnO nanoparticle size distribution, solubility, and surface energy. ACS nano, 3(7), 1703-1710.

Shifu, C., Lei, C., Shen, G., and Gengyu, C. (2006). The preparation of coupled SnO_2/TiO_2 photocatalyst by ball milling. Materials Chemistry and Physics, 98(1), 116-120.

Shifu, C., Sujuan, Z., Wei, L., and Wei, Z. (2008). Preparation and activity evaluation of p–n junction photocatalyst NiO/TiO_2. Journal of Hazardous Materials, 155(1-2), 320-326.

Söhnel, O., and Mullin, J. W. (1982). Precipitation of calcium carbonate. Journal of Crystal Growth, 60(2), 239-250.

Tai, C. Y., and Chen, F. B. (1998). Polymorphism of $CaCO_3$, precipitated in a constant-composition environment. AIChE Journal, 44(8), 1790-1798.

Tizro, A. T., and Kamali, M. (2016). Synthesis of Ag-doped $PbTiO_3$ nanoparticles: feasibility study of its decolorization of simulated methyl orange dye wastewater. Journal of Materials Science: Materials in Electronics, 27, 8613-8618.

Tracy, S. L., Williams, D. A., and Jennings, H. M. (1998). The growth of calcite spherulites from solution: II. Kinetics of formation. Journal of Crystal Growth, 193(3), 382-388.

Voicu, G., Oprea, O., Vasile, B. S., and Andronescu, E. (2013). Photoluminescence and Photocatalytic Activity of Mn-Doped ZnO Nanoparticles. Digest Journal of Nanomaterials & Biostructures (DJNB), 8(2), 667 - 675.

Wahab, R., Ansari, S. G., Kim, Y. S., Seo, H. K., and Shin, H. S. (2007). Room temperature synthesis of needle-shaped ZnO nanorods via sonochemical method. Applied Surface Science, 253(18), 7622-7626.

Wang, J., Sun, S., Pan, L., Xu, Z., Ding, H., and Li, W. (2019). Preparation and properties of $CaCO_3$-supported nano-TiO_2 composite with improved photocatalytic performance. Materials, 12(20), 3369.

Wang, R., Jiang, G., Wang, X., Hu, R., Xi, X., Bao, S., and Chen, W. (2012). Efficient visible-light-induced photocatalytic activity over the novel Ti-doped BiOBr microspheres. Powder technology, 228, 258-263.

Wang, Y., Zhang, C., Bi, S., and Luo, G. (2010). Preparation of ZnO nanoparticles using the direct precipitation method in a membrane dispersion micro-structured reactor. Powder Technology, 202(1-3), 130-136.

Wang, Z., Huang, B., Dai, Y., Qin, X., Zhang, X., Wang, P., and Yu, J. (2009). Highly photocatalytic ZnO/In_2O_3 heteronanostructures synthesized by a coprecipitation method. The Journal of Physical Chemistry C, 113(11), 4612-4617.

Wu, C., Shen, L., Yu, H., Huang, Q., and Zhang, Y. C. (2011). Synthesis of Sn-doped ZnO nanorods and their photocatalytic properties. Materials Research Bulletin, 46(7), 1107-1112.

Wu, C., Shen, L., Zhang, Y. C., and Huang, Q. (2011). Solvothermal synthesis of Cr-doped ZnO nanowires with visible light-driven photocatalytic activity. Materials Letters, 65(12), 1794-1796.

Yang, G., Yan, Z., and Xiao, T. (2012). Low-temperature solvothermal synthesis of visible-light-responsive S-doped TiO_2 nanocrystal. Applied Surface Science, 258(8), 4016-4022.

Yu, J., and Yu, X. (2008). Hydrothermal synthesis and photocatalytic activity of zinc oxide hollow spheres. Environmental science & technology, 42(13), 4902-4907.

Zhang, Y., Ram, M. K., Stefanakos, E. K., and Goswami, D. Y. (2012). Synthesis, characterization, and applications of ZnO nanowires. Journal of Nanomaterials, 2012, 1-22.

Zhao, L., Chen, X., Wang, X., Zhang, Y., Wei, W., Sun, Y., and Titirici, M. M. (2010). One-step solvothermal synthesis of a carbon@ TiO_2 dyade structure effectively promoting visible-light photocatalysis. Advanced Materials, 22(30), 3317.

Zhong, J., zhang Li, J., Lu, Y., yang He, X., Zeng, J., Hu, W., and cheng Shen, Y. (2012). Fabrication of Bi^{3+}-doped ZnO with enhanced photocatalytic performance. Applied Surface Science, 258(11), 4929-4933.

CURRICULUM VITAE

Personal Information

Name andSurname : Maher Jawad Kadhim KADHIM

Education

MSc	Çankırı Karatekin University Graduate School of Natural and Applied Sciences Department of Chemical Engineering	2020-2023
Undergraduate	University of Technology in Iraq Department of Chemical Engineering	2002-2006

WorkExperience

Year	Institution	Position
2008-Present	Iraqi Ministry of Oil	Operation engineer

AcademicActivities

1. Maher Jawad Kadhim KADHIM, Muhammed Bora AKIN, (2022). Production and Characterization of Nano-Sized Calcium Carbonate-Zinc Oxide Composites, The 1st International Karatekin Science and Technology Conference, 1-3 September 2022, Çankiri, Turkey (Full-text, oral presentation).